Flash carbonization route to magnetic carbon fiber sheet derived from cellulose paper for the bidirectional removal of dye pollutant from wastewater

Cong Han, Zhigang Jia*, Rui Chang, Mingxin Qin, Min Li, Jingjing Fang, Daqin Zhang

School of Chemistry and Chemical Engineering, Anhui University of Technology, No. 59 Hudong Road, Ma'anshan 243002, Anhui Province, China, Tel. +86-555-2311551; Fax: +86-555-2311882; emails: zjchemyue@126.com (Z. Jia), 1035584983@qq.com (C. Han), 3433458952@qq.com (R. Chang), 455010297@qq.com (M. Qin), 2021187290@qq.com (M. Li), 467972825@qq.com (J. Fang), 498819089@qq.com (D. Zhang)

ABSTRACT

Magnetic carbon fiber sheet (MCP) has been successfully prepared by novel one-step flash carbonization and magnetization method using cellulose paper as carbon source and iron(III) chloride and manganese chloride as magnetic source. The as-prepared MCP is systematically characterized by Fourier-transform infrared spectroscopy, X-ray diffraction, field emission scanning electron microscopy, nitrogen physical adsorption (BET) and thermal gravimetric analysis. Congo red (CR) and methylene blue (MB) are employed as the typical anionic and cationic probe pollutant to assess the adsorption performance of the as-prepared MCP, respectively. The adsorption results from aqueous media using a batch technique show that the adsorption can be well described by the pseudo-second-order kinetic and Langmuir isotherm models for anionic CR and cationic MB. The estimated thermodynamic constants indicated that the adsorption is a spontaneous, endothermic process. The maximum adsorption capacity values reach 245 and 140 mg g^{-1} for CR and MB, respectively. The flash carbonization and synchronous magnetization with cellulose paper can be anticipated to be a good route for resource utilization of wastepaper.

Keywords: Cellulose paper; Flash carbonization; Magnetic carbon fiber sheet; Adsorption

1. Introduction

Water is the source of life, and is also the necessary element for the industrial and agricultural activity. However, with the rapid development of global industrialization, plenty of organic pollutants are discharged into water circulation system and water pollution has become a tricky problem. Organic dyes in industrial wastewater resulted from the textile, paper, plastic, and leather industries are harmful to aquatic life and human health due to their toxic, mutagenic and carcinogenic characteristics. Dye pollutants with the biological resistance and chemical stability can hardly be metabolized by the organism.

Moreover, these dye pollutants have high water solubility and their continuous transportation in water systems can cause serious threat for the water security [1,2].

After the endeavor of many years for seeking the various techniques for relieving the water pollution, adsorption method is widely considered as the most versatile and effective method due to its advantages of simple operation, low processing cost and less secondary pollution [3–6]. Adsorption material with low cost, high adsorption capacity and easy separation is the key, which affect whether the adsorption method can be applied in the practical water treatment [7–10]. In recent years, magnetic carbon adsorbent materials have attracted intensive interest because of

* Corresponding author.

their high specific surface area, fast recovery, easy regeneration and recycle for economic and practical applications. The magnetic carbon adsorbents as one of the promising wastewater treatment materials show the excellent performance for the removal of inorganic ions and organics from aqueous solution [11–16].

Magnetic carbon can be prepared by the thermal decomposition of the single precursor containing Fe(Ni) ion, or the combination of magnetic particle with activated carbon by codeposition, or the carbonization of the polymer and biomass with magnetic materials [17–20]. The preparation of carbon is important for the low-cost and high performance magnetic absorbent for the purpose of the practical use. Combination of pyrolysis with activation is the classical synthetic methodology of activated carbon. Pyrolysis is usually performed at 600°C–900°C under an oxygen-free atmosphere with the companion of the release of gaseous products and the formation of graphitic aromatic rings rearrangement of residual carbon atoms. The subsequent activation process is to produce the ideal pore structure [21–25]. For this kind of classical carbonization strategy, some harsh condition including inert atmosphere supply and high carbonization temperature is required for the carbonization of precursors. At the same time, toxic and erosion reagents are also necessary for the high surface area. Therefore, a simple, timesaving and scalable method is indispensable for the preparation of new carbon materials.

Wastepaper as biomass waste is massively present in daily life. The main components of paper are carbohydrate and consist of 90%–99% cellulose fibers. The cellulose fiber of wastepaper is rich in carbon, pore structure and functional groups, which makes it to be an ideal carbon precursor material [26,27]. Zhu et al. [28] reported a magnetic carbon fabric synthesized by using cotton fabric as the renewable and advanced material carbon precursor via microwave-assisted heating at 750°C. Functional mesoporous carbon materials for supercapacitors and lithium-ion batteries are developed from print paper and filter paper. Wastepaper is also employed as carbon source to one-step synthesize dimensional (3D) net-like magnetic mesoporous carbon for as a renewable adsorbent [29]. However, carbonization of wastepaper needs pyrolysis of long time in nitrogen atmosphere.

Wastepaper with cellulose as main component has high water absorption, low ignition point, and is easy to be lighted in room temperature, which inspire us whether magnetic carbon can be obtained by flash carbonization with the wastepaper as the precursor. In this study, filter paper is employed as a precursor for the preparation of carbon fiber networks. Iron(III) chloride and manganese chloride are used to endow the carbon fiber magnetism by flash carbonization. Most importantly, magnetic carbon fibers are prepared by the direct flash carbonization method that can be completed in several minutes. The quick combustion method supplies a novel route for the carbonization of wastepaper. Methylene blue (MB) and congo red (CR) are the typical cationic dye category and anion dye category, respectively. Both kinds of dyes have many industrial applications and also cause negative impacts for environment. In the current work, MB and CR are employed as model pollutant to evaluate the adsorption of the as-prepared magnetic carbon fibers. The adsorption behavior and mechanisms are investigated. Kinetics, equilibrium adsorption parameters are evaluated and discussed in detail.

2. Experimental section

2.1. Preparation of paper-derived magnetic carbon fiber sheet

Magnetic carbon fiber sheet is prepared by immersion and flash carbonization method. The waste filter paper is used as the precursor of carbon fiber sheet. First, 1 mmol of $MnCl_2$ and 2 mmol $FeCl_3$ are added into 50 mL of deionized water in 200 mL breaker until the salts are completely dissolved, 2.5 g of the dried filter paper (CP) is immersed into the above-mentioned solution, and the open beaker was put in an 80°C oven until the paper became dry with the complete evaporation of water, and the immersed cellulose paper by salt solution was named as ICP. Finally, the dried ICP is ignited with lighter in air atmosphere. When cooling to the room temperature, the burnt residue is collected for further use. The as-obtained paper-based magnetic carbon materials are denoted as MCP. The detailed process can be depicted in Fig. 1.

2.2. Characterization

X-ray diffraction (XRD) patterns are obtained using X-ray powder diffraction (D8ADVANCE, Bruker Corporation, Germany) with Cu Kα radiation (λ = 1.541874 Å) in a range of $10° \leq 2\theta \leq 80°$. Scanning electron microscopy (SEM) and transmission electron microscopy (TEM) images are acquired with JSM-6490LV scanning electron microscope (Japan) and JEM-2100 transmission electron microscopy, respectively. The N_2 adsorption and desorption isotherm of the samples were observed by using a Mike ASAP 2460 gas adsorption apparatus. Thermogravimetric analysis was performed using DTG-60H thermal analyzer with the heating temperature from 25°C to 800°C at the heating rate: 10°C min^{-1}. Fourier-transform infrared spectroscopy (FTIR) spectra are collected on a Nexus FTIR spectrophotometer (Thermo Fisher, USA) in the wave number range of 400–4,000 cm^{-1}.

2.3. Batch adsorption test

CR and MB are employed as the typical anionic and cationic probe of dyes in aqueous solution. The adsorption kinetic experiments: 0.020g MCP adsorbent is added into 50 mL of dye solution (CR:80 mg/L; MB:40 mg/L) and the mixture is subjected to constant-temperature shaking at 298 K. The dye concentration is measured on a UV-vis spectrophotometer at each predetermined time point. The adsorption isotherms of CR and MB are carried out by a batch of equilibration experiments by adding the 20 mg MCP into 50 mL of the probe aqueous solution with various concentration (MB, C_0: 10–120 mg L^{-1}; CR: 20–250 mg L^{-1}) for 120 min shaking. The adsorption capacity of the dye probe is calculated by the following equation:

$$q_t = \frac{(C_0 - C_t)V}{W} \tag{1}$$

where C_0 (mg L^{-1}) and C_e (mg L^{-1}) are initial and residual concentration of dye solution, respectively; m (g) is the mass of the MCP adsorbent; V (mL) is the total volume of the dye solution.

3. Results and discussion

3.1. Characterization of the as-prepared magnetic carbon fiber sheet

The appearance transformation of CP to MCP can be easily observed during the preparation process and recorded by photograph. When lighted by lighter, the pure CP will almost completely burn and only a little of ashes is left (inset) as shown in Fig. 2a. When immersing CP into MnCl$_2$ and FeCl$_3$ solution, CP turns into light yellow color (Fig. 2b), indicating the adsorption of metal ion into the cellulose fiber of CP. As shown in Fig. 2c, MCP can be obtained through the combustion of ICP in several minutes and no any powder was produced, suggesting the fibrous structure of CP is still maintained. Furthermore, the as-prepared MCP can be firmly attracted by a magnet (Fig. 2d), which indicated the formation of magnetic component in the MCP. The detailed
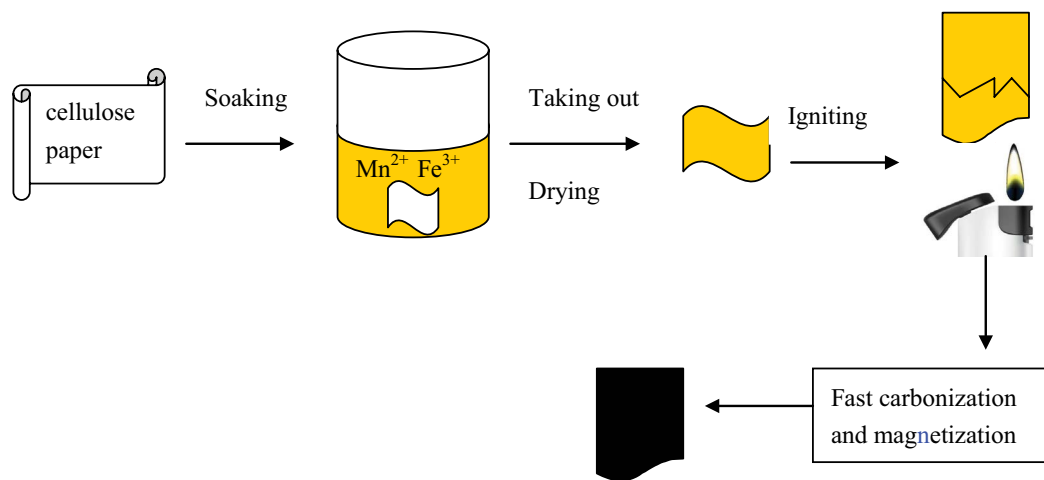

Fig. 1. Synthesis process of carbon paper prepared by flash carbonization.
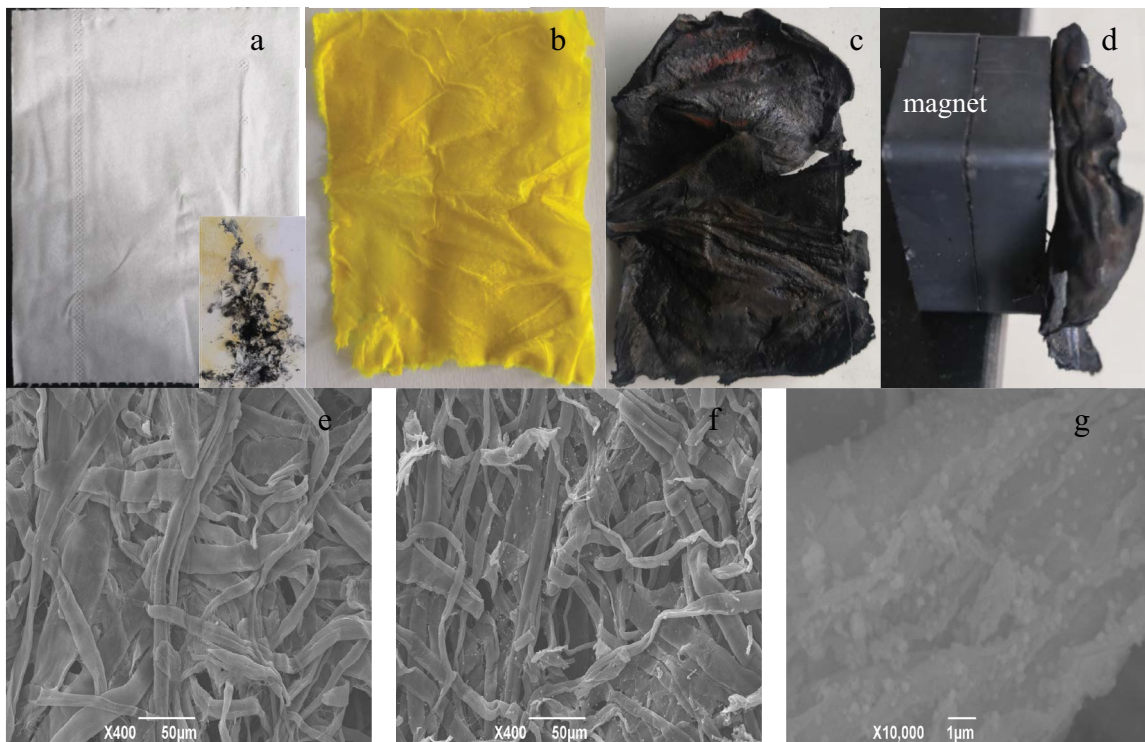

Fig. 2. Photographs of cellulose paper (a), immersed cellulose paper (b), magnetic carbon paper (c) and magnetic carbon paper attracted by a magnet (d); SEM images of pure cellulose paper (e) and magnetic carbon paper (f, g).

texture of pure CP and MCP was further shown in Figs. 2a and 1b, respectively. Long micrometer-sized fibers of pure CP criss-cross and weave into a sheet. After flash carbonization by fire, the texture of the paper well maintained and criss-crossed fibers can also be clearly seen. No powder or the disintegration of sheet was observed. However, the sheet of MCP has lost the flexible property and is apt to break up into small sheet. Furthermore, magnified image shows that many small particles adhere to the surface of the fiber (Fig. 2g) and the particles were inferred as magnetic particles. EDS analysis shows the atom ratio of Mn, Fe and O is 0.95:2.06:4.12.

In order to further understand the combustion of CP and ICP, thermogravimetric-differential thermal analysis (TG-DTA) analyses of CP and ICP are conducted and the corresponding curves are shown in Fig. 3a. There are two weight losses in TG curve of ICP. One endothermic peak and one exothermic peak correspondingly occur in the DTA curve. The first weight loss occurs at the temperature range of 50°C–100°C with the weight loss of 4.8%, which is caused by the evaporation of water in the sample with a weak endothermic peak. The second weight loss occurs at the temperature range of 200°C–300°C with the weight loss of about 65.1% with a distinguished exothermic peak. Compared with DTA curve, one endothermic peak of CP at the temperature range of 50°C–100°C is similar to that of ICP and one exothermic peak is at the temperature range of 300°C–400°C, indicating that the immersing cellulose paper

with $MnCl_2$ and $FeCl_3$ lowered the combustion point of cellulose paper and promote the combustion process. Moreover, on obvious weigh loss in TG curve or exothermic peak in DTA curve ascribed to the change of $MnCl_2$ and $FeCl_3$ can be detected. Therefore, we speculate that the reaction of $MnCl_2$ and $FeCl_3$ may occur during the combustion of cellulose paper at the temperature range of 200°C–300°C.

The phase information of the samples is investigated by XRD measurement as shown in Fig. 3b. The characteristic diffraction peaks located at 29.9°, 35.4°, 43.1°, 56.9° and 62.5°can be well indexed to (220), (311), (400), (511) and (440) crystal faces of the cubic spinel structured $MnFe_2O_4$ (JCPDS card no. 10-0319) [30]. The broad diffraction peak around 2θ = 24° corresponds to the (002) carbon phase of carbonized paper and the carbon framework exhibits the poor graphitic phase with the partially amorphous structure [31]. Another weak peaks (101) reflections plane centered at 43° is not clearly observed, which may be ascribed to the overlay with the diffraction peak with (400) of $MnFe_2O_4$ phase. These two weak peaks also indicate the amorphous nature of carbonized paper in the as-prepared MCP.

The functional groups of the as-prepared material are identified by FTIR spectroscopy. As shown in Fig. 3c, the broad band around 3,410 cm^{-1} is attributed to the stretching vibration of a large number of O–H groups. The band appearing at 1,615 cm^{-1} is due to C=C stretching vibrations of aromatic ring and representative of graphite [32]. The peak that appeared at 1,380 cm^{-1} may belong to the
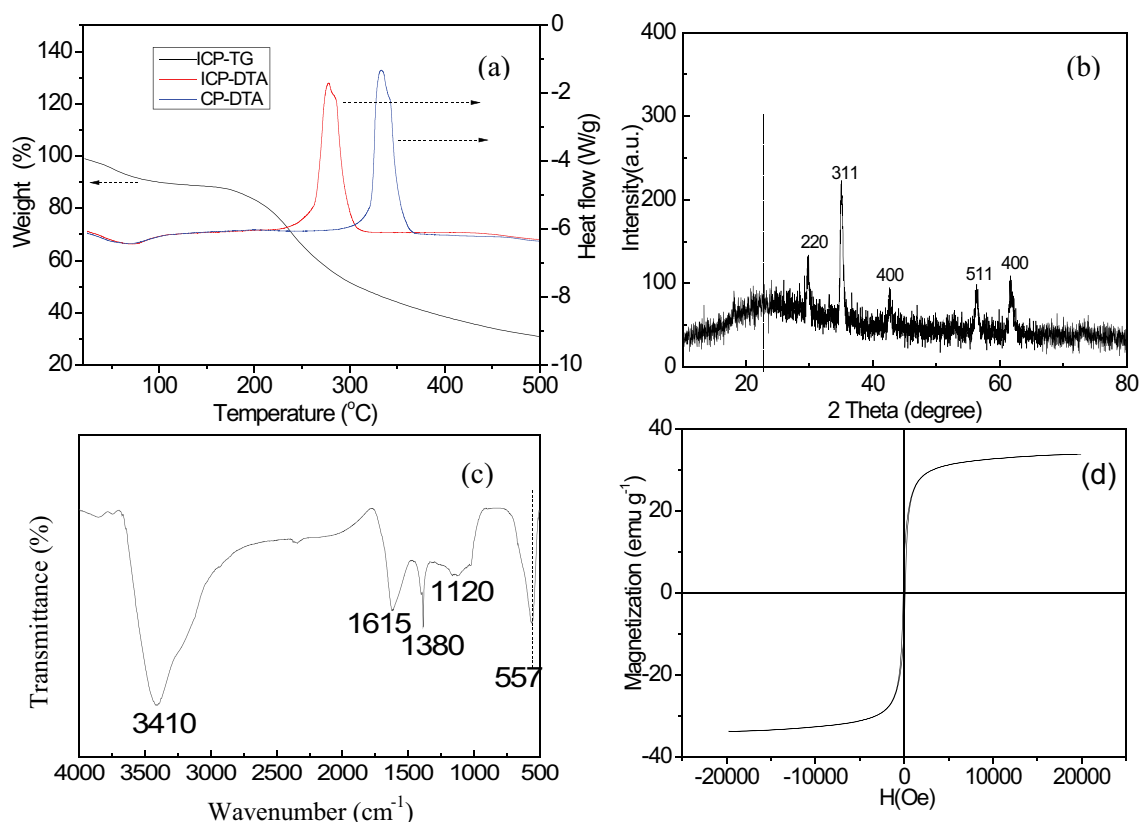

Fig. 3. TG-DTA analysis of immersed cellulose paper and DTA analysis of dried filter paper (a); X-ray diffraction patterns of magnetic carbon fiber sheet (MCP) (b); Fourier-transform infrared spectroscopy spectra of MCP (c); magnetization curve of MCP (d).

stretching vibration of the COO group in the carboxylic groups [33]. The absorption band at 1,120 cm^{-1} can be attributed to C–O stretching vibration in a carbonyl group, indicating the presence of oxygen in MCP [34]. The band at 576 cm^{-1} is caused by the intrinsic vibrations of octahedral coordinated metal ions in the spinel structure.

The magnetic behavior of MCP was investigated using the vibrating sample magnetometer. The magnetization curve is shown in Fig. 3d. Saturation magnetization value of MCP is 33.8 emu g^{-1}. The higher magnetization of the MCP is attributed to MnFe$_2$O$_4$ phase in MCP. Thus, MCP can be magnetically separated from solution by using a simple magnet.

Surface areas and porosity distributions of MCP are analyzed from the experimental data by N$_2$ physisorption. As shown in Fig. 4a, MCP presents type IV adsorption isotherms with representative H$_4$-type hysteresis loops according to IUPAC classification. A sharp increase at the lower relative pressure region is attributed to the presence of a large quantity of micropores (<2 nm). The hysteresis loop at medium-pressure zone indicates the formation of some mesoporous structures. The hysteresis loop of the samples suggests the presence of a mesoporous structure [35]. The specific surface area calculated by the BET method is up to 132.1 m^2 g^{-1}. Pore size distribution curve as shown in Fig. 4b suggests the existence of plenty of

microporous structure with average pore size of 2 nm and some mesoporous structures with the pore diameter in the range of 5–10 nm. The formation of porous structure can be ascribed to the removal of small molecules during the process of combustion of CP. On the other hand, white smokes during the combustion may be also responsible for the generation of porous structure. TEM image of MCP is shown in Fig. 4c. The randomly oriented pores of the as-prepared MCP can also be observed from the TEM image, which is in accord with N$_2$ adsorption–desorption isotherm.

3.2. Adsorption property of MCP

CR and MB dyes are selected as cationic and anionic probe pollutants for adsorption studies, respectively. The adsorption capacity of organic dyes onto MCP with the contact time is shown in Figs. 5a and b, respectively. It can be seen that adsorption capacities of CR and MB dyes onto MCP are increased with the increasing contact time. The equilibrium can be reached at 80 and 120 min for both CR and MB dye, respectively. Furthermore, the adsorption capacity of CR adsorption onto MCP rapidly increases and reaches 100 mg g^{-1} in the initial 20 min, and then holds a slow increase in the subsequent 60 min. For MB adsorption onto MCP, the adsorption capacity climbs to 65.10 mg/g in a relatively quick style in the initial
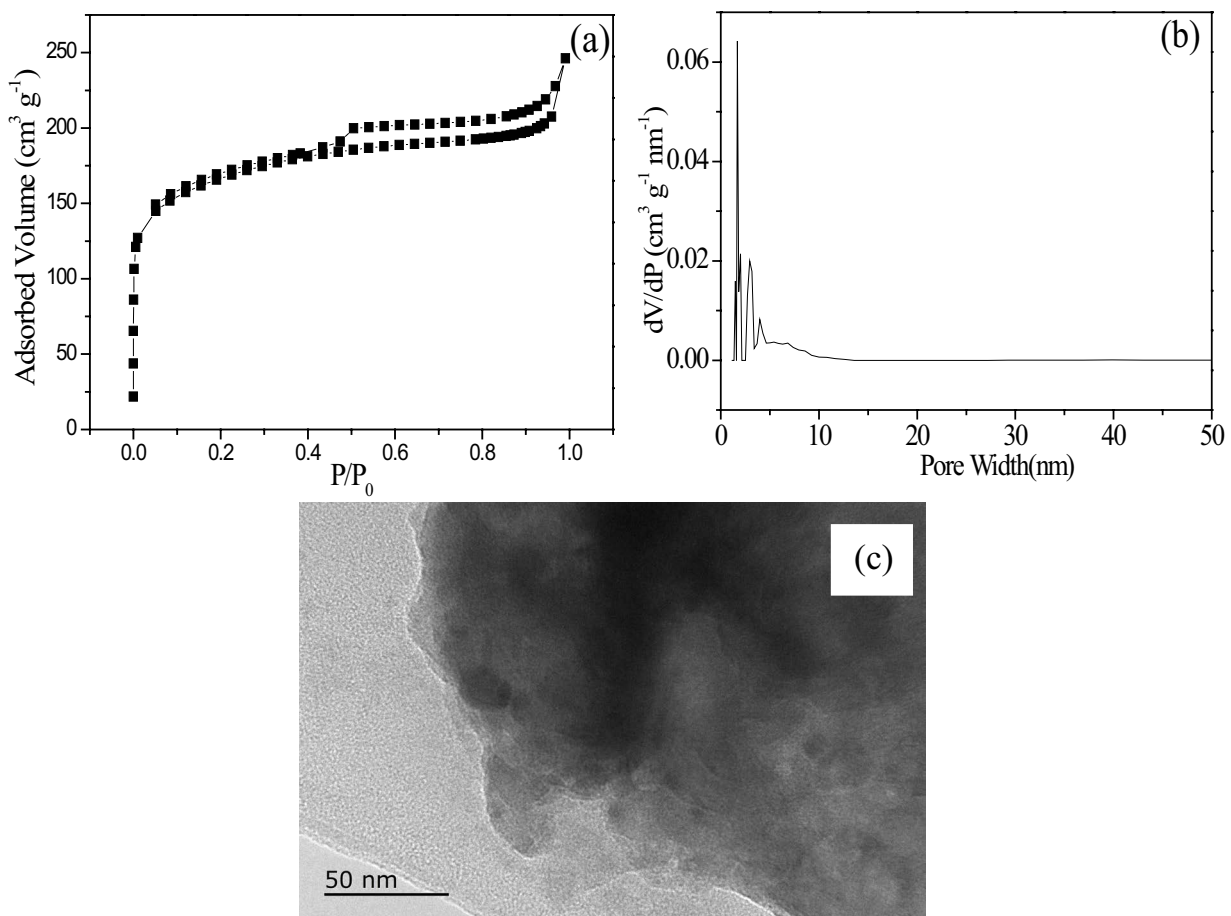

Fig. 4. N$_2$ adsorption–desorption isotherm (a), pore size distribution (b) and TEM image of magnetic carbon fiber sheet (c).
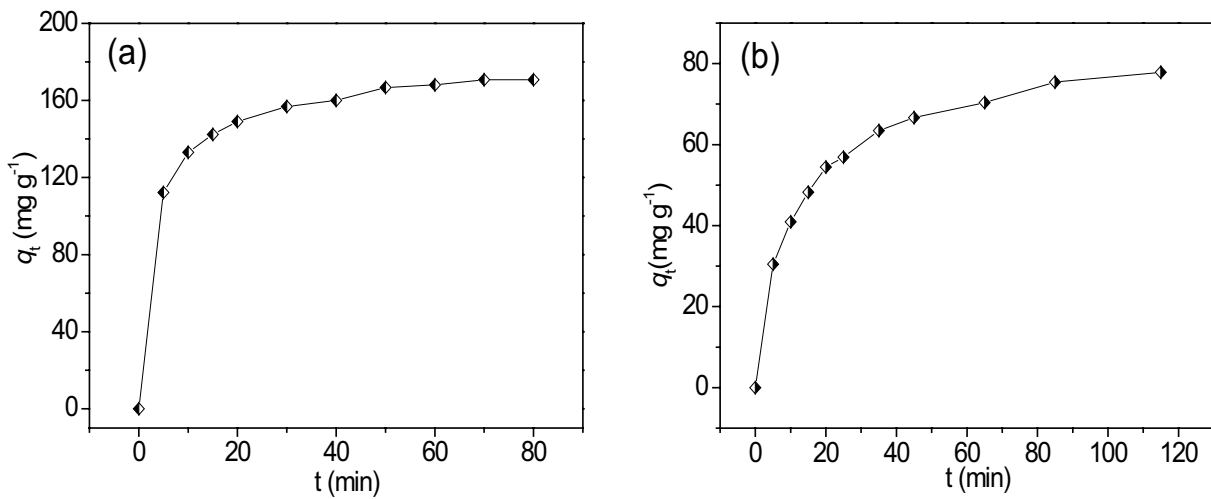
Fig. 5. Effect of contact time on the Congo red (a) and methylene blue (b) removal by magnetic carbon fiber sheet.

40 min until equilibrium is slowly achieved after subsequent 80 min. Rapid increase of adsorption capacity in the initial period can be ascribed to the amount of available vacant active sites on adsorbent surface, and the continuous reduction of adsorptive active sites with increasing contact time results in the extended equilibrium time.

To understand the adsorption mechanisms of anionic CR and cationic MB dyes onto MCP, the Lagergren pseudo-first-order and Lagergren pseudo-second-order as two well-known kinetic models are employed to investigate the adsorption kinetics. The linear forms of the pseudo-first-order model (2) and pseudo-second-order model (3) are generally expressed as follows:

$$\log\left(q_e - q_t\right) = \log\left(q_e\right) - \frac{k_1}{2.303}t \tag{2}$$

$$\frac{t}{q_t} = \frac{1}{k_2 q_e^2} + \frac{t}{q_e} \tag{3}$$

where q_e and q_t are the sorption capacities at equilibrium and at time t, respectively (mg g^{-1}). K_1 and K_2 are the pseudo-first-order and the pseudo-second-order rate constants, respectively. For the anionic CR and cationic MB adsorption onto MCP, the calculated q_e value and rate constants can be acquired from the linear fitting of pseudo-first-order equation and the pseudo-second-order equation. The fitting curves are shown in Fig. 6. Furthermore, the calculated parameters are given in Table 1. As can be seen from the above results, the high value of correlation coefficient ($R^2 > 0.99$) of pseudo-second-order kinetic model than that of the pseudo-first-order model indicates that the adsorption of two types of dye molecule with opposite charge by MCP follows pseudo-second-order kinetics, which is further testified by the good agreement of the calculated adsorption capacity ($q_{e,cal}$) of the pseudo-second-order model with the experimental adsorption capacity ($q_{e,exp}$). These suggest that chemisorption refers

to the major adsorption mechanism for anionic CR and cationic MB adsorption onto MCP [36,37].

The adsorption capacities of CR and MB onto MCP in different initial concentration and variable adsorption temperature are shown as Figs. 7a and b, respectively. It can be seen that the adsorption capacity (q_e) increases with the increasing initial concentrations and reaches relatively stable value at higher concentration. The adsorption capacities of CR onto MCP increase with the higher adsorption temperature. While, the decreasing adsorption capacities of MB onto MCP occurs with the increasing adsorption temperature.

The adsorption equilibrium studies of MB and CR are simulated by Langmuir and Freundlich model. Linear Freundlich and Langmuir isotherm model are expressed as follows:

Freundlich isotherm model

$$\log q_e = \log K_F + \frac{1}{n}\log C_e \tag{4}$$

Langmuir isotherm model

$$\frac{C_e}{q_e} = \frac{C_e}{q_m} + \frac{1}{K_L q_m} \tag{5}$$

where K_F and n are the Freundlich isotherm constants, q_e (mg g^{-1}) is the observed lead(II) adsorption capacity and C_e (mg L^{-1}) is the equilibrium concentration. q_m (mg g^{-1}) are the observed and maximum lead(II) adsorption capacities and K_L (L mg^{-1}) is the equilibrium constant related to energy of adsorption. The fitting curves are plotted as show in Fig. 8. The calculated isotherm parameters and the correlation coefficients of the experimental data are given in Table 2. According to correlation coefficients (R^2) obtained from the linear form of equations and calculated isotherm parameters (Table 2), the Langmuir isotherm equation has better conformity with the experimental data than Freundlich model. The
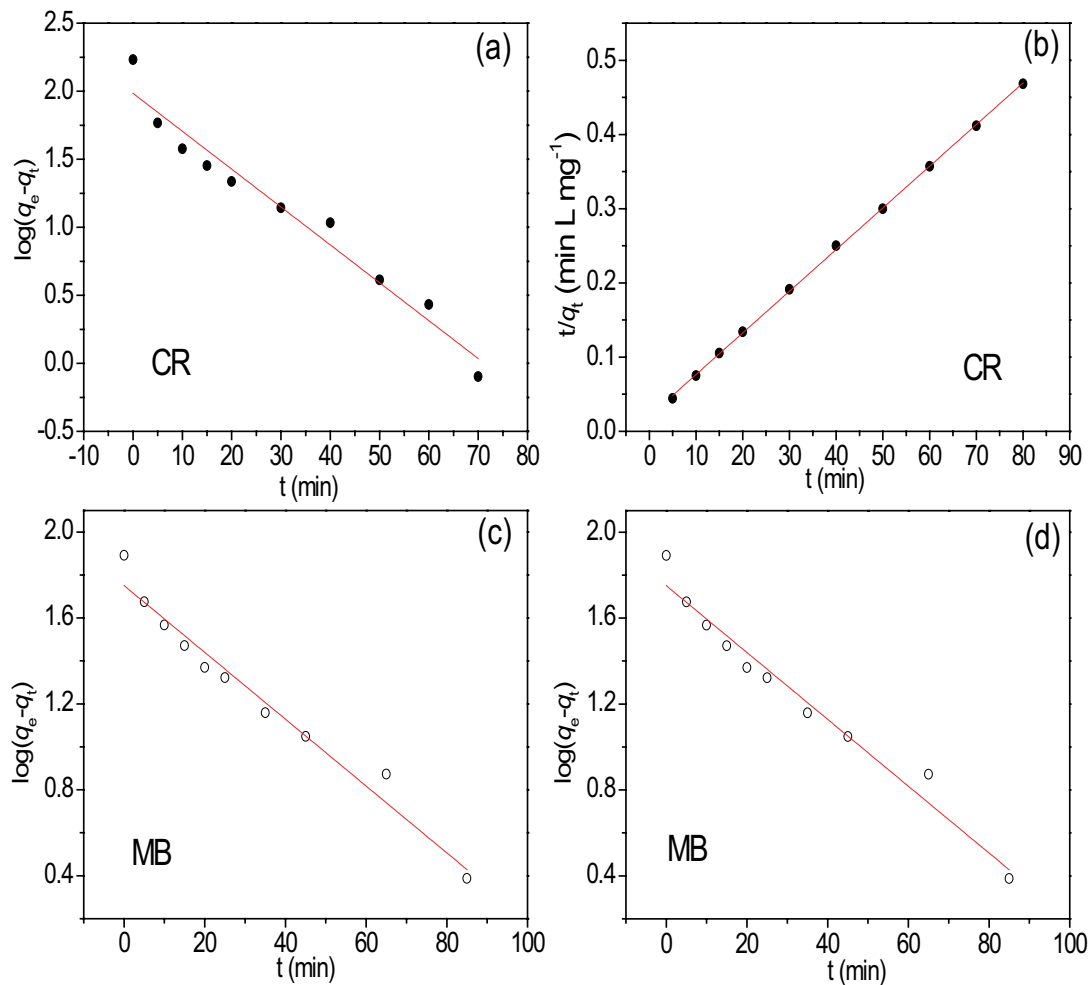
Fig. 6. Adsorption kinetic models onto magnetic carbon fiber sheet: pseudo-first-order for Congo red (CR) and methylene blue (MB) (a, c) and pseudo-second-order for CR and MB (b, d).

Table 1
Kinetic parameters for adsorption of CR and MB dye onto MCP.

Model	Pseudo-first-order model				Pseudo-second–order model		
	$q_{e,exp}$ (mg g^{-1})	$q_{e,cal}$ (mg g^{-1})	k_1 (min^{-1})	R^2	$q_{e,cal}$ (mg g^{-1})	k_2 (g mg^{-1} min^{-1})	R^2
CR	171	96.5	0.0641	0.957	178	0.0015	0.999
MB	78.1	56.4	0.0358	0.966	84.6	0.0011	0.999

CR: Congo red; MB: methylene blue.

calculated maximum adsorption capacities from Langmuir model ($q_{m,cal}$) are close to the experimental values ($q_{m,exp}$). These results suggest monolayer coverage of CR or MB dye on the surface of MCP. Furthermore, the favorability of the adsorption process of CR and MB dye on the MCP adsorbent is investigated using dimensionless separation factor (R_L) derived from the Langmuir equation:

$$R_L = \frac{1}{(1 + K_L C_0)} \tag{6}$$

where C_0 is the initial dye concentration (mg L^{-1}) and K_L is the Langmuir constant (L mg^{-1}). According to the above equation, the calculated value of R_L as shown in Table 2 is in the range of 0 and 1 for CR and MB, indicating the Langmuir adsorption of anionic CR and cationic MB on the MCP adsorbent is all favorable and the monolayer adsorption process dominates the adsorption process [38,39].

3.3. Thermodynamic analysis

Thermodynamic parameters such as the enthalpy change ($\Delta H°$, kJ mol^{-1}), the entropy change ($\Delta S°$, J mol^{-1} K^{-1}) and the
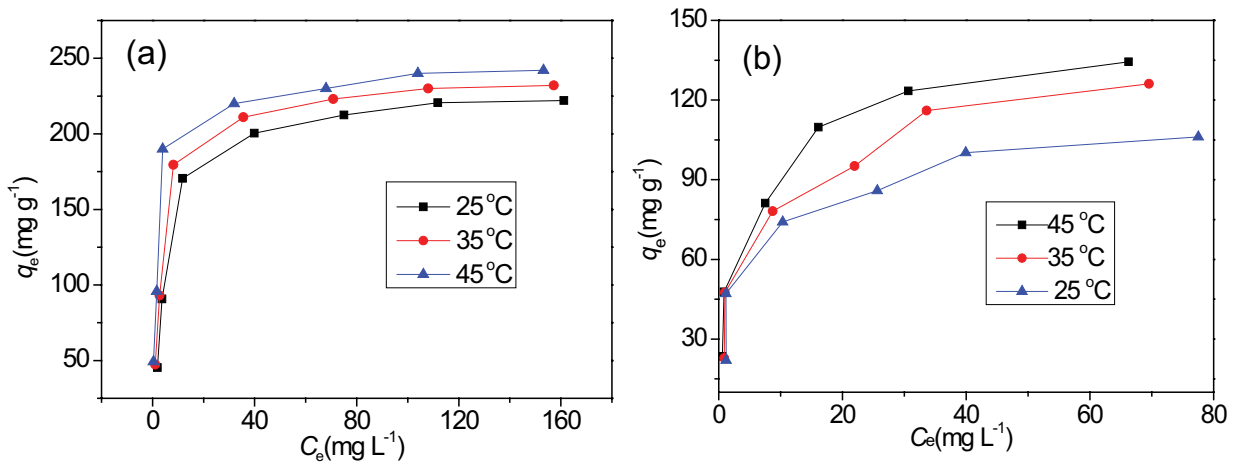
Fig. 7. Adsorption isotherms of Congo red (a) and methylene blue (b) onto magnetic carbon fiber sheet at various adsorption temperatures (25°C, 35°C and 45°C).
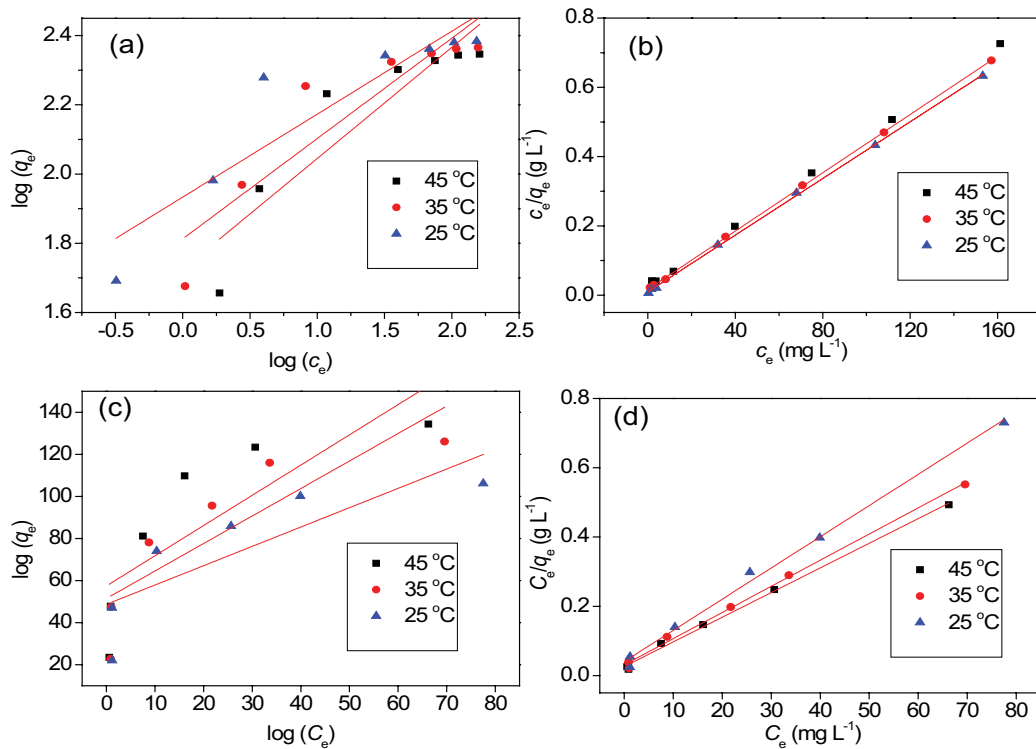

Fig. 8. Adsorption isotherm of Congo red onto the as-prepared magnetic carbon fiber sheet (MCP) simulated by the Langmuir isotherm models (a), and Freundlich isotherm models (b); Adsorption isotherm of MB onto the as-prepared MCP simulated by the Langmuir isotherm models (c), and Freundlich isotherm models (d).

Gibbs free energy change ($\Delta G°$, kJ mol^{-1}) of dye adsorption are calculated using below mentioned expressions to investigate the thermodynamic behavior:

$$K_d = \frac{q_e}{C_e} \tag{7}$$

$$\Delta G° = -RT \ln K_d \tag{8}$$

$$\ln K_d = -\frac{\Delta H°}{RT} + \frac{\Delta S°}{R} \tag{9}$$

where R is the gas constant (8.314 J mol^{-1} K^{-1}), T is solution temperature (K), C_e is the concentration of compound at equilibrium (mg L^{-1}) and q_e is the amount adsorbed at equilibrium at a particular temperature (mg g^{-1}).

$\Delta G°$ is calculated according to Eqs. (1) and (2). $\Delta H°$ and $\Delta S°$ can be calculated from the plot of $\ln K_d$ vs. $1/T$ as

Table 2
Adsorption isotherm parameters for adsorption of CR and MB dye onto MCP

Model		Langmuir model				Freundlich model		
		q_m (mg g^{-1})	K_L (L mg^{-1})	R_L	R^2	K_F (mg g^{-1})(L mg^{-1})$^{1/n}$	$1/n$	R^2
CR	25°C	231	0.168	0.023–0.229	0.999	53.0	3.12	0.807
	35°C	238	0.253	0.0156–0.165	0.999	64.9	3.45	0.816
	45°C	245	0.431	0.0092–0.104	0.999	85.8	4.17	0.817
MB	25°C	111	0.223	0.0360–0.310	0.995	31.9	0.302	0.903
	35°C	133	0.242	0.0333–0.293	0.998	35.2	0.347	0.943
	45°C	140	0.274	0.0296–0.268	0.996	38.3	0.337	0.952

shown in Fig. 9. All the obtained thermodynamic parameters are listed in Table 3. The negative values of $\Delta G°$ indicated the spontaneous nature of adsorption process of CR and MB onto MCP. For adsorption of CR dye, the Gibbs free energy decreases with increasing the temperature, indicating the adsorption of CR adsorption onto MCP is favorable. Positive $\Delta H°$ and $\Delta S°$ values suggest the endothermic nature and the increasing randomness at the solid–liquid interface, respectively. While, for MB dye adsorption, the increasing Gibbs free energy with the raised temperature and the negative values of $\Delta H°$ explained the exothermic behavior for this process and lower temperature is more favorable for the adsorption. The negative value of $\Delta S°$ implies the randomness decreased at the solid–liquid interface during the process of cationic MB adsorption onto MCP.

The used adsorbent for CR adsorption and MB adsorption is further characterized by XRD and FTIR technique. As shown in Fig. 10a, the powder X-ray diffraction (PXRD) patterns of the used adsorbent reveal that the characteristic peaks are in agreement with that of the unused adsorbent and graphitic carbon discerned by the weak and wide peak at 24.5° still exists in the samples, which indicate that the adsorbent material is stable in water environment and has potential application prospect for the treatment of wastewater. FTIR spectra of MCP after the adsorption of MCP for MB is shown in Fig. 10b, the band at around 3,400 cm^{-1} assigned to O–H shifts to higher wavenumbers, indicating that the H-bond interaction and the ion exchange process between MB and the MCP may contribute to the adsorption

[40]. The weak band at 1,620 cm^{-1}, assigned to the C=C vibration, shifted to a lower wavenumber of 1,595 cm^{-1}. For the adsorption of CR onto MCP, the weak band at 1,620 cm^{-1} of the C=C vibration shifts to 1,610 cm^{-1}. The blue shift of C=C vibration may result from the π–π stacking between aromatic moieties of carbon material and dye molecules [41]. The new bands of 2,920 and 2,850 cm^{-1} as displayed in Fig. 10c are assigned to the C–H bond stretching vibrations of CR and MB molecule absorbed onto the surface of MCP [42].

The effect of pH for the adsorption capacity is investigated. As shown in Fig. 10d, adsorption capacity is not obviously influenced with the pH variation from 2 to 12, and their adsorption capacity value fluctuated in the range of 150–172 and 74.1–81.0 mg g^{-1} for anionic CR and cationic MB. The as-prepared MCP can effectively remove the anionic CR and cationic MB in a wide pH range. However, pH$_{PZC}$ values of MCP are 4.12 according to pH drift method (Fig. S1). The pH value of the suspension of CR (80 mg/L) and MB (40 mg/L) solution is measured to be 8.52 and 6.71, which indicates the negative charges on the surface of MCP. This result showed that adsorption can mainly be ascribed to π–π stacking between aromatic moieties of carbon material and dye molecules besides electrostatic interaction. On the other hand, the higher adsorption temperature promotes the motion of dye molecule and makes high contact chance between CR (MB) molecule and MCP adsorbent, which enhances the adsorption capacity of CR(MB) through π–π stacking between aromatic moieties of MCP and CR(MB) dye molecules.
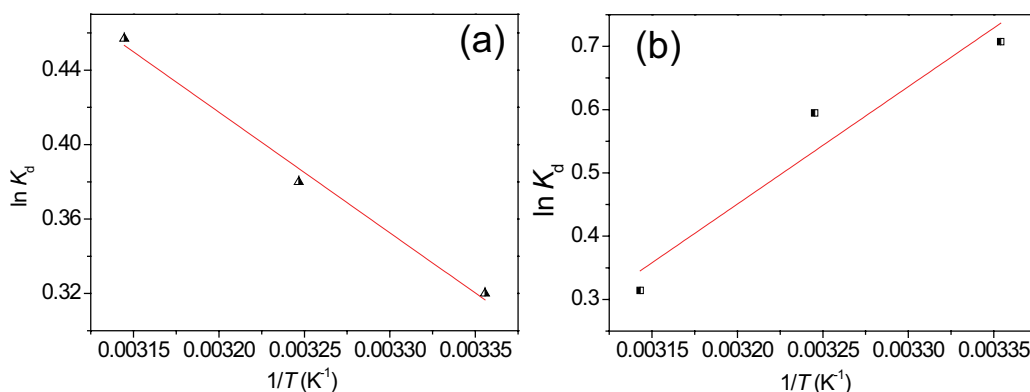
Fig. 9. Van't Hoff plot for adsorption of Congo red and methylene blue dye onto magnetic carbon fiber sheet.

Table 3
Thermodynamic parameters for adsorption of CR and MB dye onto MCP

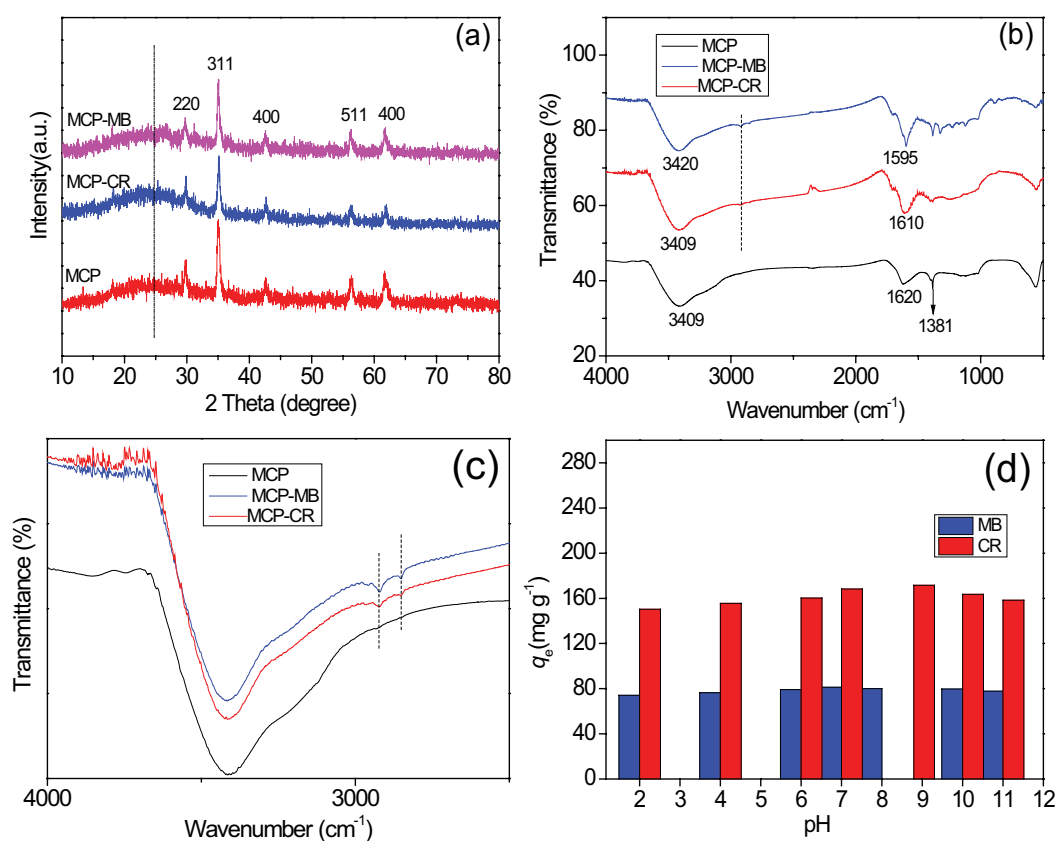|	Adsorption temperature (°C)	$\Delta G°$ (kJ mol^{-1})	$\Delta H°$ (kJ mol^{-1})	$\Delta S°$ (J K^{-1} mol^{-1})
CR	298	−0.793	5.39	20.7
	308	−0.997		
	318	−1.21		
MB	298	−1.75	−15.4	−45.6
	308	−1.52		
	318	−0.831		

CR: Congo red; MB: Methylene blue.

Fig. 10. X-ray diffraction patterns (a), Fourier-transform infrared spectroscopy (FTIR) spectra (b) and the enlarged FTIR spectra (c) of the unused magnetic carbon fiber sheet (MCP) and used MCP for Congo red (CR) and methylene blue (MB) adsorption and adsorption capacity of CR and MB onto MCP with various pH.

Plenty of adsorbents have been developed for the removal of anionic or cationic dye. Quite a few adsorbents modified by the specific functional group, such as carboxy- and amino-group, can only selectively remove anionic or cationic dye. The adsorption capacity is greatly influenced by pH of the solution, which can only acquire high removal effect in acidic or alkali condition. It is well known that the practical wastewater to be disposed is complex and there are different types of pollutants. In our study, the as-prepared MCP adsorbent shows excellent adsorption performance in wide pH range. The comparison of the maximum adsorption capacity of the MCP adsorbent with the other adsorbents previously reported for the bidirectional adsorption of dyes is listed in Table 4. As can be seen, the adsorption capacity of the prepared adsorbent is in the range of 231–245 mg g^{-1} for anionic CR dye and 111–140 mg g^{-1} for the cationic MB dye at 25°C–45°C. The results in this table showed that the magnetic MCP adsorbent can be effectively used for the bidirectional removal of anionic and cationic dye from aqueous solution. MCP without any modification is superior to other magnetic carbon due to one-step flash carbon-

Table 4
Comparison of the adsorption for CR and MB onto MCP and the reported magnetic carbons

Adsorbent	Adsorbate	Maximum adsorption capacity	Temp. (K)	Reference
Eucalyptus wood-based magnetic activated carbon (MAC)	MB	228.22 mg g^{-1}	298–328 K	[43]
Hierarchical magnetic porous carbon fibers (MBFs)	MB	143.0 mg g^{-1}		[44]
Core-shell functionalized magnetic activated carbons	MB	182.45 mg g^{-1}		[45]
MOPC*x* nanomaterials	MB	124.1 mg g^{-1}		[46]
Graphene–Fe$_3$O$_4$@carbon (GFC) hybrids	MB	73.26 mg g^{-1}		[47]
Magnetic graphene oxide (MGO)	MB	70.0 mg g^{-1}		[48]
Poly(acrylic acid)/Magnetic graphene oxide (PAA/MGO)		290.7 mg g^{-1}		
Magnetic graphene-carbon nanotube composite	MB	65.79 mg g^{-1}		[49]
MCP	MB	111–140	298–318 K	This work
Bamboo hydrochars	CR	22.7 mg g^{-1}		[50]
Gold-magnetic nanocomposite loaded on activated carbon	CR	43.88 mg g^{-1}		[51]
Titanium oxide (TiO$_2$) nanoparticles (NPs) loaded onto activated carbon (AC)	CR	14.7 mg L^{-1}		[52]
AmMAC2	CR	189.39 mg L^{-1}		[53]
Biochars	CR	8.0–22.6 mg L^{-1}		[54]
Magnesium and silica coated magnetized palm shell activated carbon (MMPAC)	CR	257.25 mg L^{-1}		[55]
MCP	CR	231–244 mg g^{-1}	298–318 K	This work

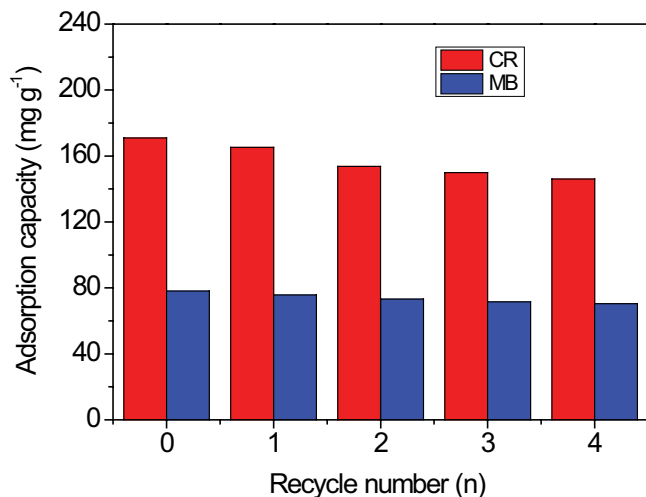MCP: Magnetic carbon fiber sheet; CR: Congo red; MB: methylene blue.

Fig. 11. Reusability of the synthesized magnetic carbon fiber sheet.

ization and magnetization with comparable performance although the adsorption capacity is not the maximum one.

The reusability of the adsorbent is an important aspect for the practical application in the treatment of wastewater. The as-prepared MCP is reused four times after continuous adsorption–desorption processes. Desorption of dyes from MCP has been performed with anhydrous ethanol as eluent. As shown in Fig. 11, the removal rate of CR and MB can still reach 85.4% and 90.2% of the initial adsorption capacity after four cycles, respectively.

4. Conclusion

In this study, magnetic carbon fiber sheet is successfully prepared by flash carbonization and magnetization. The common paper is used as the carbon source to prepare carbon adsorption material, and magnetic MnFe$_2$O$_4$ particles are synchronous formed at the surface of carbon fiber sheet using the infiltrating iron(III) chloride and manganese chloride as the source. Magnetic carbon fiber sheet is the partly graphene carbon with MnFe$_2$O$_4$ particles and possesses oxygen-rich functional groups. Anionic CR and cationic MB as probe pollutants are employed to assess the adsorption property of MCP. The results revealed that the adsorption process for the anionic CR and cationic MB followed the pseudo-second-order kinetic and Langmuir isotherm models, and the adsorption is spontaneous and physisorption process. The as-prepared MCP showed an excellent ability for anionic dye and cationic dye in wide pH range, indicating π–π stacking between aromatic moieties of carbon material and dye molecules has more contribution besides the H-bond interaction and the ion exchange. The as-prepared materials are expected to be useful in the wastewater treatment containing dye. The quick one-step synthesis strategy of carbonization and magnetization is quite promising for other carbon materials. Wastepaper in our daily life can be recycled and reused by this way.

References

[1] A.G.B. Pereira, F.H.A. Rodrigues, A.T. Paulino, A.F. Martins, A.R. Fajardo, Recent advances on composite hydrogels designed for the remediation of dye-contaminated water and wastewater: a review, J. Clean. Prod., 17 (2020) 124703.

[2] X. Zhou, Y.X. Zhou, J.S. Liu, S. Song, J.J. Sun, J.H. Zhu, H.P. Gong, L. Wang, C.W. Wu, M.F. Li, Study on the pollution characteristics and emission factors of PCDD/Fs from disperse dye production in China, Chemosphere, 228 (2019) 328–334.

[3] S.S. Li, L. Huang, H.J. Zhang, Z. Huang, Q.L. Jia, S.W. Zhang, Adsorption mechanism of methylene blue on oxygen-containing functional groups modified graphitic carbon spheres: experiment and DFT study, Appl. Surf. Sci., 28 (2021) 148386.

[4] Z.C. Li, H. Hanafy, L. Zhang, L. Sellaoui, M.S. Netto, M.L.S. Oliveira, M.K. Seliem, G.L. Dotto, A.B. Petriciolet, Q. Li, Adsorption of congo red and methylene blue dyes on an ashitaba waste and a walnut shell-based activated carbon from aqueous solutions: experiments, characterization and physical interpretations, Chem. Eng. J., 388 (2020) 124263.

[5] K.L. Yu, X.J. Lee, H.C. Onge, W.h. Chen, J.S. Chang, C.S. Lin, P.L. Show, T.C. Lin, Adsorptive removal of cationic methylene blue and anionic Congo red dyes using wet-torrefied microalgal biochar: Equilibrium, kinetic and mechanism modeling, Environ. Pollut., 3 (2020) 115986.

[6] S. Parvin, B.K. Biswas, M.A. Rahman, M.H. Rahman, M.S. Anik, M.R. Uddin, Study on adsorption of Congo red onto chemically modified egg shell membrane, Chemosphere, 236 (2019) 124326.

[7] F. Zarekarizi, A. Morsali, Ultrasonic-assisted synthesis of nano-sized metal-organic framework: a simple method to explore selective and fast Congo Red adsorption, Ultrason. Sonochem., 69 (2020) 105246.

[8] H.J. Hu, J.Y. Liu, Z.H. Xu, Z.Y. Zhang, B. Cheng, W.K. Ho, Hierarchical porous Ni/Co-LDH hollow dodecahedron with excellent adsorption property for Congo red and Cr(VI) ions, Appl. Surf. Sci., 478 (2019) 981–990.

[9] J. Liu, N. Wang, H.L. Zhang, J. Baeyens, Adsorption of Congo red dye on FexCo$_{3-x}$O$_4$ nanoparticles, J. Environ. Manage., 238 (2019) 473–483.

[10] Z.Q. Cheng, Z.W. Wang, P.C. Wu, Y.H. Wang, J.W. Fu, Mass fabrication of oxygen and nitrogen co-doped 3D hierarchical porous carbon nanosheets by an explosion-assisted strategy for supercapacitor and dye adsorption application, Appl. Surf. Sci., 529 (2020) 147079.

[11] J.H. Li, L.S. Huang, X.Q. Jiang, L.X. Zhang, X.S. Sun, Preparation and characterization of ternary Cu/Cu$_2$O/C composite: an extraordinary adsorbent for removing anionic organic dyes from water, Chem. Eng. J., 404 (2021) 127091.

[12] P. Sirjudheen, P. Karthikeyan, K. Ramkumar, Magnetic carbon-biomass from the seeds of *Moringa oleifera*@MnFe$_2$O$_4$ composite as an effective and recyclable adsorbent for the removal of organic pollutants from water, J. Mol. Liq., 21 (2020) 114829.

[13] P. Li, D.T. Hua, J.S. Huang, J.J. Tang, P.J. Zhang, F. Meng, Development of magnetic porous carbon nano-fibers for application as adsorbents in the enrichment of trace Sudan dyes in foodstuffs, J. Chromatogr. A, 1625 (2020) 461305.

[14] W.Y. Gu, X.Y. Huang, Y.H. Tian, M. Cao, L. Zhou, Y. Zhou, J. Lu, J.Y. Lei, Y.B. Zhou, L.Z. Wang, Y.D. Liu, J.L. Zhang, High-efficiency adsorption of tetracycline by cooperation of carbon and iron in a magnetic Fe/porous carbon hybrid with effective Fenton regeneration, Appl. Surf. Sci., 538 (2021) 147813.

[15] P. Ying, Q.J. Ding, B.H. Li, X.X. Wang, Y.W. Liu, J.H. Chen, F. Ke, J.Q. Liu, Self-adjusted bimetallic zeolitic-imidazolate framework-derived hierarchical magnetic carbon composites as efficient adsorbent for optimizing drug contaminant removal, Chemosphere, 263 (2021) 128101.

[16] Y. Cui, L. Qing, W.W. Kang, J.H. Ma, Y.Z. Yang, X.G. Liu, Magnetic carbon nanospheres: synthesis, characterization,

[17] H.R. Yuan, Y.P. Wang, B. Suo, Dielectric relaxation and magnetic resonance of nitrogen-doped graphene-coated FeNi nanoparticles on nitrogen-doped carbon nanosheets, J. Alloys Compd., 854 (2021) 157212.

[18] W.G. Zhao, Y.M. Tian, X.X. Chu, S. Zhang, H.G. Dong, F. Yan, C.L. Zhu, Y.J. Chen, Preparation and characteristics of a magnetic carbon nanotube adsorbent: its efficient adsorption and recoverable performances, Sep. Purif. Technol., 257 (2021) 117917.

[19] W.F. Zhao, X. Jing, Y.Q. Tian, C.P. Feng, Magnetic Fe$_3$O$_4$@ porous activated carbon effervescent tablet-assisted deep eutectic solvent-based dispersive liquid–liquid microextraction of phenolic endocrine disrupting chemicals in environmental water, Microchem. J., 159 (2020) 105416.

[20] Y.F. Li, A.R. Zimmerman, F. He, J.J. Chen, L.J. Han, H. Chen, X. Hu, B. Gao, Solvent-free synthesis of magnetic biochar and activated carbon through ball-mill extrusion with Fe$_3$O$_4$ nanoparticles for enhancing adsorption of methylene blue, Sci. Total Environ., 722 (2020) 137972.

[21] Z. Li, Y.J. Cao, G.Y. Li, L. Chen, W.Y. Xu, M.J. Zhou, B.H. He, W. Wang, Z.H. Hou, High rate capability of S-doped ordered mesoporous carbon materials with directional arrangement of carbon layers and large d-spacing for sodium-ion battery, Electrochim. Acta, 366 (2021) 137466.

[22] F. Zhang, S. Zong, Y. Zhang, H.J. Lv, X.Y. Liu, J. Du, A.B. Chen, Preparation of hollow mesoporous carbon spheres by pyrolysis-deposition using surfactant as carbon precursor, Power Sour., 27 (2020) 229274.

[23] C. Ma, L.Q. Wu, M. Dirican, H. Cheng, J.J. Li, Y. Song, J.L. Shi, X.W. Zhang, ZnO-assisted synthesis of lignin-based ultra-fine microporous carbon nanofibers for supercapacitors, J. Colloid Interface Sci., 27 (2020) 2563.

[24] W.Q. Zou, S.K. Zhang, Y. Abbas, W. Liu, Y.H. Zhang, Z.P. Wu, B. Xu, Structurally designed heterochain polymer derived porous carbons with high surface area for high-performance supercapacitors, Appl. Surf. Sci., 530 (2020) 147296.

[25] M. Kim, H. Lim, X.T. Xu, M.S.A. Hossain, J.B. Na, N.N. Awaludin, J. Shah, L.K. Shrestha, K. Airga, A.K. Nanjundan, D.J. Martin, J.G. Shapter, Y. Yamauchi, Sorghum biomass-derived porous carbon electrodes for capacitive deionization and energy storage, Microporous Mesoporous Mater., 1 (2020) 110757.

[26] M. Shahrousvand, F.A. Tabar, E. Shahrousvand, A. Babaei, M.M. Hasani-Sadrabadi, G.M.M. Sadeghi, H. Jafari, A. Salimi, High aspect ratio phospho-calcified rock candy-like cellulose nanowhiskers of wastepaper applicable in osteogenic differentiation of hMSCs, Carbohydr. Polym., 175 (2017) 293–302.

[27] J. Yu, D.H. Zhang, S.K. Zhu, P. Chen, G.T. Zhu, X.T. Jiang, S.Y. Di, Eco-friendly and facile one-step synthesis of a three dimensional net-like magnetic mesoporous carbon derived from wastepaper as a renewable adsorbent, RSC Adv., 22 (2019) 12419–12427.

[28] J.H. Zhu, H.B. Gu, J. Guo, M.J. Chen, H.G. Wei, Z.P. Luo, H.A. Colorado, M. Yerra, D.W. Ding, T.C. Ho, N. Haldolaarachchige, J. Hopper, D.P. Young, Z.H. Guo, S.Y. Wei, Mesoporous magnetic carbon nanocomposite fabrics for highly efficient Cr(VI) removal, J. Mater. Chem. A, 7 (2014) 2256–2265.

[29] H. Argun, G. Onaran, Hydrogen gas production from waste paper by sequential dark fermentation and electrohydrolysis, Int. J. Hydrogen Energy, 41 (2016) 8057–8066.

[30] G.S. Wang, Y.Z. Zeng, F. Zhou, X. Chen, Y.Y. Ma, L.Y. Zheng, M.X. Li, Y. Sun, X.Y. Liu, H.Y. Liu, One-step solvothermal synthesis of porous MnFe$_2$O$_4$ nanoflakes and their magnetor-heological properties, J. Alloys Compd., 819 (2020) 153044.

[31] D.J. Li, X.L. Cheng, R. Xu, Y. Wu, X.F. Zhou, C. Ma, Y. Yu, Manipulation of 2D carbon nanoplates with a core–shell structure for high-performance potassium-ion batteries, J. Mater. Chem. A, 7 (2019) 19929–19938.

[32] Z.M. Shen, J. Du, Y.H. Mo, A.B. Chen, Nanocomposites of reduced graphene oxide modified with mesoporous

carbon layers anchored by hollow carbon spheres for energy storage, Carbon, 173 (2021) 22–30.

[33] C.J. Chen, S. Mi, D.M Lao, P.P. Shi, Z.F. Tong, Z.X. Li, H.Y. Hu, Single-step synthesis of eucalyptus sawdust magnetic activated carbon and its adsorption behavior for methylene blue, RSC Adv., 9 (2019) 22248–22262.

[34] T.J. Chen, J. Zhang, Z.Q. Wang, R.D. Zhao, J.J. He, J.H. Wu, J.G. Qin, Oxygen-enriched gasification of lignocellulosic biomass: syngas analysis, physicochemical characteristics of the carbon-rich material and its utilization as an anode in lithium ion battery, Energy, 212 (2020) 118771.

[35] W.M. Du, Z.R. Zhang, L.G. Du, X.Y. Fan, Z.W. Shen, X.R. Ren, Y.P. Zhao, C.Z. Wei, S.H. Wei, Designing synthesis of porous biomass carbon from wheat straw and the functionalizing application in flexible, all-solid-state supercapacitors, J. Alloys Comp., 797 (2019) 1031–1040.

[36] J.L. Wang, X. Guo, Adsorption kinetic models: physical meanings, applications, and solving methods, J. Hazard. Mater., 390 (2020) 122156.

[37] C.C. Li, D. Chen, J. Ding, Z.P. Shi, A novel hetero-exopolysaccharide for the adsorption of methylene blue from aqueous solutions: isotherm, kinetic, and mechanism studies, J. Clean. Prod., 265 (2020) 121800.

[38] A.M. Osmana, A.H. Hendi, T.A. Saleh, Simultaneous adsorption of dye and toxic metal ions using an interfacially polymerized silica/polyamide nanocomposite: kinetic and thermodynamic studies, J. Mol. Liq., 314 (2020) 113640.

[39] T.A. Saleh, Nanocomposite of carbon nanotubes/silica nanoparticles and their use for adsorption of Pb(II): from surface properties to sorption mechanism, Desal. Wat. Treat., 57 (2016) 10730–10744,

[40] S.S. Yang, Y.D. Chen, J.H. Kang, T.R. Xie, L. He, D.F. Xing, R.Q. Ren, S.H. Ho, W.M. Wu, Generation of high-efficient biochar for dye adsorption using frass of yellow mealworms (larvae of *Tenebrio molitor* Linnaeus) fed with wheat straw for insect biomass production, J. Clean. Prod., 227 (2019) 33–47.

[41] K. Gupta, D. Gupta, O.P. Khatri, Graphene-like porous carbon nanostructure from Bengal gram bean husk and its application for fast and efficient adsorption of organic dyes, Appl. Surf. Sci., 476 (2019) 647–657.

[42] Z.G. Jia, Z.Y. Li, T. Ni, S.B. Li, Adsorption of low-cost absorption materials based on biomass (*Cortaderia selloana* flower spikes) for dye removal: kinetics, isotherms and thermodynamic studies, J. Mol. Liq., 229 (2017) 285–292.

[43] X. Alvarez, Á. Cancela, A. Rodríguez, E. Valero, Á. Sanchez, Green filters of *Eucalyptus globulus* for microalgae harvesting from freshwater reservoir and reuse of biomass harvested for pellet production, Process Saf. Environ., 147 (2021) 497–504.

[44] C. Bao, J.J. Ma, L.C. Zhou, Y.M. Shao, Q. Wu, F. Wang, Self-template synthesis of hierarchical magnetic porous carbon fibers derived from Fe(BTC)-coated bamboo fibers for fast removal of methylene blue, RSC Adv., 106 (2015) 87616–87625.

[45] H. Ebadollahzadeh, M. Zabihi, Competitive adsorption of methylene blue and Pb (II) ions on the nano-magnetic activated carbon and alumina, Mat. Chem. Phys., 248 (2020) 122893.

[46] T.V. Tran, D.T.C. Nguyen, H.T.N. Le, C.D. Duong, L.G. Bach, H-T.T. Nguyen, T.D. Nguyen, Facile synthesis of manganese oxide-embedded mesoporous carbons and their adsorbability towards methylene blue, Chemosphere, 227 (2019) 455–461.

[47] M. Khan, M.M. Tahir, S.F. Adil, H.U. Khan, M.R.H. Siddiqui, A.A. Al-warthan, W. Tremel, Hybridization of graphene sheets and carbon-coated Fe_3O_4 nanoparticles as a synergistic adsorbent of organic dyes, J. Mater. Chem. A, 22 (2012) 25108–25115.

[48] J.W. Zhang, M.S. Azam, C. Shi, Poly(acrylic acid) functionalized magnetic graphene oxide nanocomposite for removal of methylene blue, RSC Adv., 5 (2015) 32272–32282.

[49] F.F. Wang, M.H. Cao, C. Wang, J. Huang, B. Yan, Q.X. Liu, H.B. Zeng, Kinetics and thermodynamics of adsorption of methylene blue by a magnetic graphene-carbon nanotube composite, Appl. Surf. Sci., 290 (2014) 116–124.

[50] Y. Li, A. Meas, S. Shan, R. Yang, X. Gai, Production and optimization of bamboo hydrochars for adsorption of Congo red and 2-naphthol. Bioresour. Technol., 207 (2016) 379–386.

[51] E.A. Dil, M. Ghaedi, A. Asfaram, A.A. Bazrafshan, Ultrasound wave assisted adsorption of congo red using gold-magnetic nanocomposite loaded on activated carbon: optimization of process parameters, Ultrason. Sonochem., 46 (2018) 99–105.

[52] N. Masoudian, M. Rajabi, M. Ghaedi, Titanium oxide nanoparticles loaded onto activated carbon prepared from biowaste watermelon rind for the efficient ultrasonic-assisted adsorption of congo red and phenol red dyes from wastewaters, Polyhedron, 173 (2019) 114105.

[53] C.H. Tian, C.H. Feng, M.Z. Wei, Y.H. Wu, Enhanced adsorption of anionic toxic contaminant Congo Red by activated carbon with electropositive amine modification, Chemosphere, 208 (2018) 476–483.

[54] J.H. Park, J.J. Wang, Y.L. Meng, Z. Wei, R, D.D. Laune, D.C. Seo, Adsorption/desorption behavior of cationic and anionic dyes by biochars prepared at normal and high pyrolysis temperatures, Colloids Surf. A, 572 (2019) 274–282.

[55] S. Kittappa, F.M. Jais, M. Ramalingam, N.S. Mohd, S. Ibrahim, Functionalized magnetic mesoporous palm shell activated carbon for enhanced removal of azo dyes, J. Environ. Chem. Eng., 8 (2020) 104081.
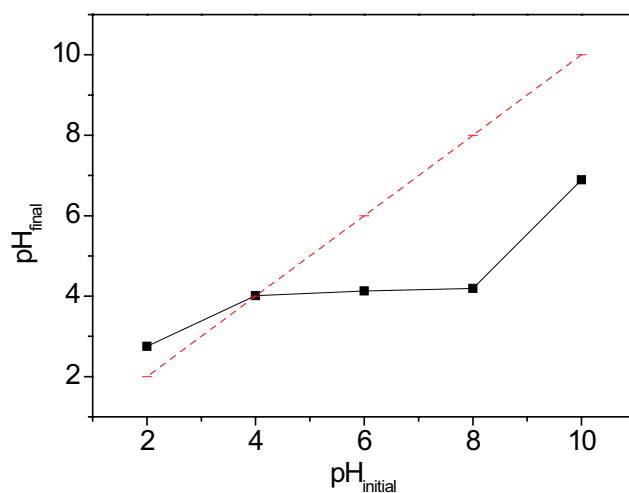
Supplementary information

Fig. S1. pH_{final} vs. $pH_{initial}$ of magnetic carbon fiber sheet.